ELSEVIER

Electrical Power and Energy Systems 28 (2006) 77–85

ELECTRICAL POWER & ENERGY SYSTEMS

www.elsevier.com/locate/ijepes

TCSC-firing angle model for optimal power flow solutions using Newton's method

Hugo Ambriz-Pérez [a,*], Enrique Acha [b], Claudio R. Fuerte-Esquivel [c]

[a] *Comisión Federal de Electricidad, México, Unidad de Ingeniería Especializada, Río Ródano No. 14- Piso 10, Sala 1002, Col. Cuauhtemoc, CP 06598 México, México*

[b] *Department of Electronics and Electrical Engineering, University of Glasgow, Rankine Building, Oakfield Avenue, G12 8LT Glasgow, Scotland, UK*

[c] *Universidad Michoacana de San Nicolás de Hidalgo (U.M.S.N.H.), División de Estudios de Posgrado, Facultad de Ingeniería Eléctrica, Ciudad Universitaria Morelia, Michoacán, México CP 58030, México*

Received 1 October 2004; accepted 20 October 2005

Abstract

A novel power flow model for the thyristor-controlled series compensator (TCSC) is presented in this paper. The model takes the form of a firing angle-dependant, nodal admittance matrix that is then incorporated in an existing optimal power flow (OPF) algorithm. Comprehensive OPF solutions of TCSC-upgraded power networks are achieved via Newton's method. The thyristor's firing angle, a newly introduced state variable in OPF formulations, is combined with the nodal voltage magnitudes and angles of the power network in a single frame-of-reference for unified, iterative solutions. This load flow TCSC model advances current models on two counts: (i) it takes full account of the loop current present in the TCSC under either partial or full conduction operating modes; (ii) only compensation regions lying outside the TCSC resonant bands are considered by the OPF solution. This new model is a more efficient counterpart than an existing TCSC controllable reactance model [1]Fuerte-Esquivel C.R., Acha E. A newton-type algorithm for the control of power flow in electrical power networks. IEEE Trans Power Deliv 1997; 2(4):1474–1480.

Keywords: FACTS; TCSC; OPF; Newton's method

1. Introduction

Electric utilities world-wide are actively considering the installation of flexible AC transmission systems (FACTS) devices with the aim of maximising active power flows across existing corridors whilst, at the same time, increasing the overall control performance of the power network [2,3]. FACTS is an umbrella title which encompasses a wide range of new power network controllers. FACTS controllers make use of the latest high-current, high-power electronics technology to ensure 'delay free', safe and accurate responses. These devices have the ability to control, in an adaptive fashion, key network parameters that have a direct bearing on the operation of the power system. Examples of these parameters are nodal voltage magnitudes and angles, transmission line impedance and active and reactive power flows. Examples of FACTS controllers are: unified power flow controllers (UPFCs), static compensators (STATCOMs), inter-phase power controllers (IPCs) and thyristor-controlled series and shunt compensators.

The TCSC is a key member of the FACTS family. It allows rapid and continuous changes of the transmission line impedance [4,5]. Active power flow across the compensated transmission line can be maintained at a specified level under a wide range of operating conditions. A schematic representation of the TCSC is shown in Fig. 1. It consists of a capacitor bank in parallel with a thyristor-controlled reactor (TCR).

A TCSC configuration, showing to be very effective is where the TCSC comprises a large number of series connected TCSC modules [4]. This TCSC configuration is termed advanced series compensator (ASC); it is reported to exert control with minimum losses and minimum harmonic distortion [4]. An alternative arrangement consists of a conventional capacitor bank of large rating in series with a TCSC of small rating at each end of the capacitor bank [5].

* Corresponding author. Tel.: +52 55 5229 4400x40207; fax: +52 55 5229 4400x40236.

E-mail addresses: hugo.ambriz@cfe.gob.mx (H. Ambriz-Pérez), eacha@elec.gla.ac.uk (E. Acha), cfuerte@zeus.umich.mx (C.R. Fuerte-Esquivel).

0142-0615/$ - see front matter © 2005 Elsevier Ltd. All rights reserved.
doi:10.1016/j.ijepes.2005.10.003

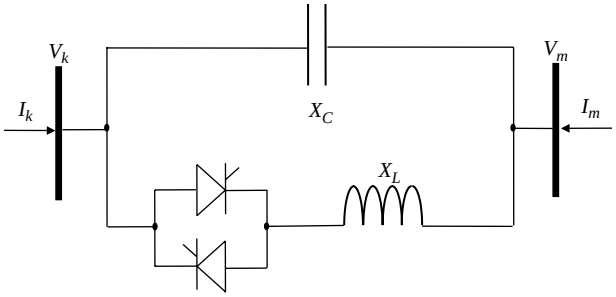

Fig. 1. TCSC module.

A closed-form expression for the fundamental frequency impedance of the TCSC module shown in Fig. 1 has been obtained elsewhere [6]. The result has been achieved by solving the ordinary differential equations involving the TCSC voltages and currents and by subjecting the intermediate result to a Fourier transform analysis. The end result is a transcendental impedance equation that is a function of the thyristor's firing angle. In this paper, the fundamental frequency impedance of the TCSC module is used as the starting point for building a flexible and robust OPF-TCSC algorithm.

A considerable amount of work relating to the TCSC has been published in the following areas: experiences of commercial operation [4,5]; performance and test models for electro magnetic transient (EMTP) and SSR mitigation studies [7,8] and power systems stability [5,9,10]. However, little progress has been reported on models and tools suitable for assessing the impact of TCSC devices on improving the steady state security and economic performance of the power network. In fact, a pioneering but limited work [11] based on linear programming and a controllable reactance may be the only publication available in open literature that addresses these two very important issues of the TCSC technology. That work, however, failed to address the very important issue of the TCSC impedance characteristic and accompanying resonant points.

This has provided the motivation for extending our Newton OPF program to encompass more advanced TCSC models. Two possible ways of representing a TCSC module exist in our program, by means of a controllable reactance and by means of the newly implemented firing angle-dependent impedance.

The former model uses the reactance as the control parameter in the OPF solution whereas the latter uses the thyristor's firing angle. The Newton OPF algorithm shows equal reliability towards the convergence with either TCSC model. However, if the controllable reactance model is used, an additional iterative process is required in order to determine the firing angle further to the power flow solution. Alternatively, if the thyristor's firing angle is used then an answer is readily available for the TCSC's firing angle upon convergence of the power flow solution. Case studies involving two standard test networks are presented to show the algorithm's flexibility and reliability towards the convergence.

2. TCSC fundamental frequency impedance

The expression for the fundamental frequency TCSC impedance, as a function of the thyristor's firing angle, is given as [4,7]:

$$X_{\mathrm{TCSC}} = -X_{\mathrm{C}} + C_1(2(\pi-\alpha) + \sin(2(\pi-\alpha))) - C_2\cos^2 \times(\pi-\alpha)[\varpi\tan(\varpi(\pi-\alpha)) - \tan(\pi-\alpha)] \quad (1)$$

where

$$X_{\mathrm{LC}} = \frac{X_{\mathrm{C}}X_{\mathrm{L}}}{X_{\mathrm{C}}-X_{\mathrm{L}}} \quad (2)$$

$$C_1 = \frac{X_{\mathrm{C}}+X_{\mathrm{LC}}}{\pi} \quad (3)$$

$$C_2 = \frac{4X_{\mathrm{LC}}^2}{X_{\mathrm{L}}\pi} \quad (4)$$

and $X_{\mathrm{C}} = 1/\omega C$ is the reactance of the capacitor bank; $X_{\mathrm{L}} = \omega L$ is the reactance of the linear inductor; α is the firing angle after capacitor voltage zero crossing; $\varpi = \omega_0/\omega$; $\omega_0 = 1/(LC)^{1/2}$ and $\omega = 2\pi f$.

Fig. 2 shows a typical, 60 Hz TCSC impedance-firing angle characteristic. The inductive and capacitive reactances are taken to be 2.6 and 15 Ω, respectively. These parameters correspond to the Kayenta TCSC scheme [4,7]. TCSCs are operated in the range of 90–180°. It can be observed that a resonance takes place when the firing angle approaches a value of 143°. In fact, for this characteristic, firing angles in the range of 140–145° would lead to high impedance operations. From the equipment design point of view, realistic TCSC-OPF models should avoid using such resonant regions as part of their solution space. Maximum and minimum TCSC firing angles in the capacitive and inductive regions are carefully established at the design stage in order to prevent the TCSC operating in high impedance regions, as this will result in high voltage drops across the TCSC [4,7]. Also, careful selection of inductive and capacitive elements should avoid the presence of multiple resonant points.

In the range of 90–180°, the TCSC resonant points are given by the following expression,

$$\alpha = \pi\left(1 - \frac{(2n-1)\omega\sqrt{LC}}{2}\right) \quad n = 1, 2, 3\ldots \quad (5)$$

From the numeric viewpoint, multiple resonant impedance points pose numerical difficulties to the OPF solution. The

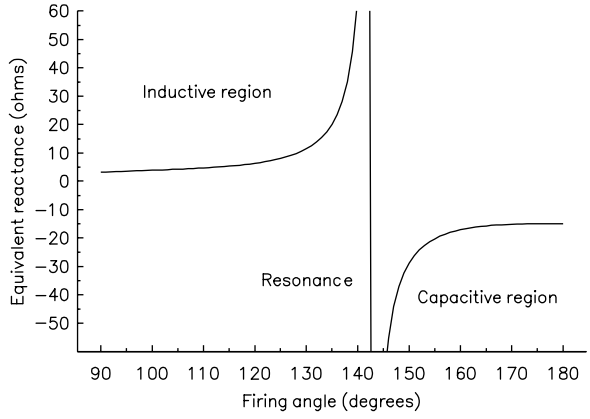

Fig. 2. TCSC steady state impedance characteristic.

numerical properties of the Jacobian and Hessian equations become severely degraded.

3. TCSC nodal power equations

The nodal power equations for the firing angle-based TCSC controller are presented below. The derivation is based on the transfer admittance matrix of the TCSC module shown in Fig. 1,

$$\begin{bmatrix} \mathbf{I}_k \\ \mathbf{I}_m \end{bmatrix} = \begin{bmatrix} jB_{kk} & jB_{km} \\ jB_{mk} & jB_{mm} \end{bmatrix} \begin{bmatrix} \mathbf{V}_k \\ \mathbf{V}_m \end{bmatrix} \tag{6}$$

where

$$B_{kk} = B_{mm} = B_{TCSC} = -\frac{1}{X_{TCSC}} \tag{7}$$

$$B_{km} = B_{mk} = -B_{TCSC} = \frac{1}{X_{TCSC}} \tag{8}$$

In the absence of resistive elements in the TCSC module, the active and reactive power equations at node k and node m may be written as follows:

$$P_k = -V_k V_m B_{TCSC} \sin(\theta_k - \theta_m) \tag{9}$$

$$Q_k = -V_k^2 B_{TCSC} + V_k V_m B_{TCSC} \cos(\theta_k - \theta_m) \tag{10}$$

$$P_m = -V_m V_k B_{TCSC} \sin(\theta_m - \theta_k) \tag{11}$$

$$Q_m = -V_m^2 B_{TCSC} + V_m V_k B_{TCSC} \cos(\theta_m - \theta_k) \tag{12}$$

where P_k, P_m, Q_k and Q_m are the active and reactive power injections at nodes k and m, respectively. V_k, V_m, θ_k and θ_m are the voltage magnitude and phase angle of nodes k and m, respectively.

4. TCSC-OPF formulation

An existing OPF algorithm has been extended to include the TCSC model presented above.

4.1. TCSC Lagrangian function

The incorporation of the TCSC power equations into an OPF algorithm using Newton's method requires that for each TCSC present in the network, the matrix **W** be augmented by two rows and two columns in cases when the TCSC is exerting active power flow control. However, if the TCSC is not controlling active power flow then matrix **W** is only augmented by one row and one column. The firing angle α is an extra state variable, which enters into the OPF formulation. In the former case, a new Lagrange multiplier is added to account for the contribution of the power flow across the branch.

The TCSC state variables are combined with the network nodal voltage magnitudes and phase angles in a single frame-of-reference for a unified optimal solution via Newton's method. The TCSC state variables are adjusted automatically so as to satisfy specified power flows, voltage magnitudes and optimality conditions as given by Kuhn and Tucker [17].

The first step in finding the optimal solution is to build a Lagrangian function corresponding to the power flow mismatch equations at nodes k and m. They are explicitly modelled in OPF Newton's method as an equality constraint given by the following equation [12,13]:

$$L_{km}(\mathbf{x},\boldsymbol{\lambda}) = \lambda_{pk}(P_k + P_{dk} - P_{gk}) + \lambda_{qk}(Q_k + Q_{dk} - Q_{gk}) + \lambda_{pm} \times (P_m + P_{dm} - P_{gm}) + \lambda_{qm}(Q_m + Q_{dm} - Q_{gm}) \tag{13}$$

where P_{dk}, P_{dm}, Q_{dk}, Q_{dm} are active and reactive power loads at nodes k and m, respectively. P_{gk}, P_{gm}, Q_{gk}, Q_{gm} are scheduled active and reactive power generations at nodes k and m, respectively. λ_{pk}, λ_{pm}, λ_{qk}, λ_{qm} are Lagrange multipliers at nodes k and m, respectively. The vector of state variables is $\mathbf{x} = [\mathbf{V\theta}]^t$, where V and θ are the voltage magnitudes and angles, respectively. The superscript t indicates transposition.

The active power flow across branch m–l in Fig. 3 is controlled by the TCSC connected between nodes k and m. In the OPF formulation, this operating condition is expressed as an equality constraint, which remains active throughout the iterative process unless one expressly wishes this constraint to be deactivated.

The operating condition is represented by the following equation,

$$L_{flow}(\mathbf{x},\boldsymbol{\lambda}) = \lambda_{ml}(P_{ml} - P_{specified}) \tag{14}$$

where λ_{ml} is the Lagrange multiplier associated with the active power flowing from node m to node l. $P_{specified}$ is the target value of active power flow across the TCSC component.

4.2. Linearised system of equations

First and second order derivative terms of Eqs. (13) and (14) are obtained and placed in matrix **W** and gradient vector **g**. The linearised system of equations for minimising the Lagrangian

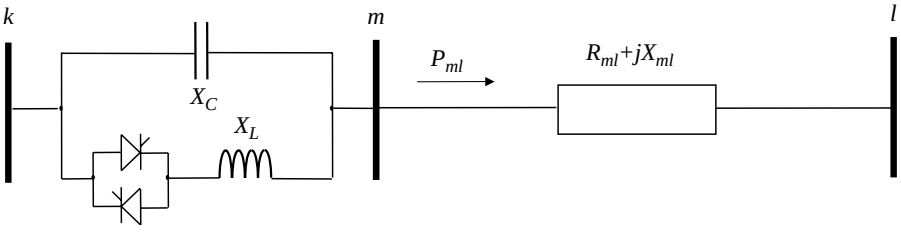

Fig. 3. Compensated transmission line.

function via Newton's method is given by,

$$\mathbf{W}\Delta\mathbf{z} = -\mathbf{g} \tag{15}$$

where matrix **W** contains second partial derivatives of the Lagrangian function $L(\mathbf{x},\lambda)$ with respect to state variables **x** and Lagrange multipliers **λ**. The gradient vector **g** is $[\nabla_{\mathbf{x}} \nabla_{\lambda}]^t$. It consists of first partial derivative terms. **Δz** is the vector of correction terms, given by $[\Delta\mathbf{x}\Delta\lambda]^t$.

An expanded version of Eq. (15), as applied to the TCSC circuit of Fig. 1 is given by Eq. (16). It must be noted that the Lagrangian, L, of the compensated branch, k–l, consists of the sum of Eqs. (13) and (14), i.e. $L = L_{\mathbf{km}}(\mathbf{x},\boldsymbol{\lambda}) + L_{\text{flow}}(\mathbf{x},\boldsymbol{\lambda})$.

The first and second derivative expressions for all the terms used in Eq. (16) are given in Appendix A. The operated in standard control mode, i.e. the TCSC is controlling active power flow from nodes m to l.

In OPF applications, lower cost solutions are obtained when the OPF algorithm itself selects the optimum level of power flow across the TCSC. Nevertheless, the TCSC model is very flexible and any change in the TCSC operating mode is easily accommodated in the general OPF formulation given in Eq. (16). For instance, if the TCSC is not controlling active power flow then matrix **W** is suitably modified to reflect this operating mode. This can be done by adding the second derivative term of a large (infinite), quadratic penalty factor to the diagonal element corresponding to multipliers λ_{ml} and by setting this multiplier to zero for the whole of the iteration process. The first derivative term of the quadratic penalty function is evaluated and added to the corresponding gradient element.

$$\begin{bmatrix}
\frac{\partial^2 L}{\partial\theta_k^2} & \frac{\partial^2 L}{\partial\theta_k\partial V_k} & \frac{\partial P_k}{\partial\theta_k} & \frac{\partial Q_k}{\partial\theta_k} & \frac{\partial^2 L}{\partial\theta_k\partial\theta_m} & \frac{\partial^2 L}{\partial\theta_k\partial V_m} & \frac{\partial P_m}{\partial\theta_k} & \frac{\partial Q_m}{\partial\theta_k} & & & & & \frac{\partial^2 L}{\partial\theta_k\partial\alpha} & & \Delta\theta_k & -\frac{\partial L}{\partial\theta_k} \\
\frac{\partial L}{\partial V_k\partial\theta_k} & \frac{\partial^2 L}{\partial V_k^2} & \frac{\partial P_k}{\partial V_k} & \frac{\partial Q_k}{\partial V_k} & \frac{\partial^2 L}{\partial V_k\partial\theta_m} & \frac{\partial^2 L}{\partial V_k\partial V_m} & \frac{\partial P_m}{\partial V_k} & \frac{\partial Q_m}{\partial V_k} & & & & & \frac{\partial^2 L}{\partial V_k\partial\alpha} & & \Delta V_k & -\frac{\partial L}{\partial V_k} \\
\frac{\partial P_k}{\partial\theta_k} & \frac{\partial P_k}{\partial V_k} & 0 & 0 & \frac{\partial P_k}{\partial\theta_m} & \frac{\partial P_k}{\partial V_m} & 0 & 0 & & & & & \frac{\partial P_k}{\partial\alpha} & & \Delta\lambda_{pk} & -\frac{\partial L}{\partial\lambda_{pk}} \\
\frac{\partial Q_k}{\partial\theta_k} & \frac{\partial Q_k}{\partial V_k} & 0 & 0 & \frac{\partial Q_k}{\partial\theta_m} & \frac{\partial Q_k}{\partial V_m} & 0 & 0 & & & & & \frac{\partial Q_k}{\partial\alpha} & & \Delta\lambda_{qk} & -\frac{\partial L}{\partial\lambda_{qk}} \\
\frac{\partial^2 L}{\partial\theta_m\partial\theta_k} & \frac{\partial^2 L}{\partial\theta_m\partial V_k} & \frac{\partial P_k}{\partial\theta_m} & \frac{\partial Q_k}{\partial\theta_m} & \frac{\partial^2 L}{\partial\theta_m^2} & \frac{\partial^2 L}{\partial\theta_m\partial V_m} & \frac{\partial P_m}{\partial\theta_m} & \frac{\partial Q_m}{\partial\theta_m} & \frac{\partial^2 L}{\partial\theta_m\partial\theta_l} & \frac{\partial^2 L}{\partial\theta_m\partial V_l} & \frac{\partial P_l}{\partial\theta_m} & \frac{\partial Q_l}{\partial\theta_m} & \frac{\partial^2 L}{\partial\theta_m\partial\alpha} & \frac{\partial P_{ml}}{\partial\theta_m} & \Delta\theta_m & -\frac{\partial L}{\partial\theta_m} \\
\frac{\partial^2 L}{\partial V_m\partial\theta_k} & \frac{\partial^2 L}{\partial V_m\partial V_k} & \frac{\partial P_k}{\partial V_m} & \frac{\partial Q_k}{\partial V_m} & \frac{\partial L}{\partial V_m\partial\theta_m} & \frac{\partial^2 L}{\partial V_m^2} & \frac{\partial P_m}{\partial V_m} & \frac{\partial Q_m}{\partial V_m} & \frac{\partial^2 L}{\partial V_m\partial\theta_l} & \frac{\partial^2 L}{\partial V_m\partial V_l} & \frac{\partial P_l}{\partial V_m} & \frac{\partial Q_l}{\partial V_m} & \frac{\partial^2 L}{\partial V_m\partial\alpha} & \frac{\partial P_{ml}}{\partial V_m} & \Delta V_m & -\frac{\partial L}{\partial V_m} \\
\frac{\partial P_m}{\partial\theta_k} & \frac{\partial P_m}{\partial V_k} & 0 & 0 & \frac{\partial P_m}{\partial\theta_m} & \frac{\partial P_m}{\partial V_m} & 0 & 0 & \frac{\partial P_m}{\partial\theta_l} & \frac{\partial P_m}{\partial V_l} & 0 & 0 & \frac{\partial P_m}{\partial\alpha} & & \Delta\lambda_{pm} & -\frac{\partial L}{\partial\lambda_{pm}} \\
\frac{\partial Q_m}{\partial\theta_k} & \frac{\partial Q_m}{\partial V_k} & 0 & 0 & \frac{\partial Q_m}{\partial\theta_m} & \frac{\partial Q_m}{\partial V_m} & 0 & 0 & \frac{\partial Q_m}{\partial\theta_l} & \frac{\partial P_m}{\partial V_l} & 0 & 0 & \frac{\partial Q_m}{\partial\alpha} & & \Delta\lambda_{qm} & -\frac{\partial L}{\partial\lambda_{qm}} \\
 & & & & \frac{\partial^2 L}{\partial\theta_l\partial\theta_m} & \frac{\partial^2 L}{\partial\theta_l\partial V_m} & \frac{\partial P_m}{\partial\theta_l} & \frac{\partial Q_m}{\partial\theta_l} & \frac{\partial^2 L}{\partial\theta_l^2} & \frac{\partial^2 L}{\partial\theta_l\partial V_l} & \frac{\partial P_l}{\partial\theta_l} & \frac{\partial Q_l}{\partial\theta_l} & & \frac{\partial P_{ml}}{\partial\theta_l} & \Delta\theta_l & -\frac{\partial L}{\partial\theta_l} \\
 & & & & \frac{\partial^2 L}{\partial V_l\partial\theta_m} & \frac{\partial^2 L}{\partial V_l\partial V_m} & \frac{\partial P_m}{\partial V_l} & \frac{\partial Q_m}{\partial V_l} & \frac{\partial L}{\partial V_l\partial\theta_l} & \frac{\partial^2 L}{\partial V_l^2} & \frac{\partial P_l}{\partial V_l} & \frac{\partial Q_l}{\partial V_l} & & \frac{\partial P_{ml}}{\partial V_l} & \Delta V_l & -\frac{\partial L}{\partial V_l} \\
 & & & & \frac{\partial P_l}{\partial\theta_m} & \frac{\partial P_l}{\partial V_m} & 0 & 0 & \frac{\partial P_l}{\partial\theta_l} & \frac{\partial P_l}{\partial V_l} & 0 & 0 & & & \Delta\lambda_{pl} & -\frac{\partial L}{\partial\lambda_{pl}} \\
 & & & & \frac{\partial Q_l}{\partial\theta_m} & \frac{\partial Q_l}{\partial V_m} & 0 & 0 & \frac{\partial Q_l}{\partial\theta_l} & \frac{\partial Q_l}{\partial V_l} & 0 & 0 & & & \Delta\lambda_{ql} & -\frac{\partial L}{\partial\lambda_{ql}} \\
\frac{\partial^2 L}{\partial\alpha\partial\theta_k} & \frac{\partial^2 L}{\partial\alpha\partial V_k} & \frac{\partial P_k}{\partial\alpha} & \frac{\partial Q_k}{\partial\alpha} & \frac{\partial^2 L}{\partial\alpha\partial\theta_m} & \frac{\partial^2 L}{\partial\alpha\partial V_m} & \frac{\partial P_m}{\partial\alpha} & \frac{\partial Q_m}{\partial\alpha} & & & & & \frac{\partial^2 L}{\partial\alpha^2} & & \Delta\alpha & -\frac{\partial L}{\partial\alpha} \\
 & & & & \frac{\partial P_{ml}}{\partial\theta_m} & \frac{\partial P_{ml}}{\partial V_m} & 0 & 0 & \frac{\partial P_{ml}}{\partial\theta_l} & \frac{\partial P_{ml}}{\partial V_l} & 0 & 0 & & 0 & \Delta\lambda_{ml} & -\frac{\partial L_{\text{flow}}}{\partial\lambda_{ml}}
\end{bmatrix} \tag{16}$$

derivative terms corresponding to inequality constraints are incorporated in matrix **W** only after state variable outside limits are detected.

Once Eq. (16) has been assembled and combined with matrix **W** and gradient vector **g** of the entire network then a sparsity-oriented solution is carried out. This process is repeated until a small, pre-specified tolerance is reached for all the variables involved. It must be remarked that this procedure corresponds to the case in which the TCSC is being

4.3. Handling limits of TCSC firing angle

In the OPF formulation, voltage magnitude and active power limits are included in the inequality constraints set. The multiplier method [18] is used to handle this set. Here, a penalty term is added to the Lagrangian function $L(\mathbf{x},\lambda)$ which then becomes the augmented Lagrangian function. Variables inside bounds are ignored whilst binding inequality constraints become part of the augmented Lagrangian function and, hence, become enforced.

The handling of the TCSC firing angle can be carried out by using the following generic function,

$$\phi_i(g_i(x),\mu_i) = \begin{cases} \mu_i(g_i(x)-\bar{g}_i)+\dfrac{c}{2}(g_i(x)-\bar{g}_i)^2 & \text{if } \mu_i + c(g_i(x)-\bar{g}_i) \geq 0 \\ \mu_i(g_i(x)-\underline{g}_i)+\dfrac{c}{2}(g_i(x)-\underline{g}_i)^2 & \text{if } \mu_i + c(g_i(x)-\underline{g}_i) \leq 0 \end{cases} \quad (17)$$

where $g_i(x)$ is the state variable value, i.e. the actual value of α, $\bar{g}$and $\underline{g}$ are the maximum and minimum limits of this state variables, i.e. upper and lower firing angle ceilings; μ is a multiplier term and c is a penalty term which adapts itself in order to force inequality constraints within limits while minimising the objective function.

Firing angle values close to a resonant point give rise to large impedance increments, which would affect adversely the good mathematical properties of Eq. (15). Fortunately, our OPF algorithm avoids incorporating resonant bands as part of the solution space. The firing angle varies in the range 90°–α_{max} in the inductive region and in the range α_{min}–180° in the capacitive region. The range α_{max}–α_{min} is a non-operative region.

5. Initial conditions

The solution process is started by assuming that the following initial conditions are used in the OPF algorithm.

5.1. Nodal voltage magnitudes and angles

The variables in vector **z** are suitably initialised in order to start the iterative process. The state variables are initialised similarly to load flow problems. 1 p.u. voltage magnitudes and 0 voltage angles provide a suitable starting condition. Engineering experience indicates that, for most practical problems, the variation of voltage magnitude and voltage angle from the 1 and 0 initial conditions is relatively small.

5.2. Active power schedule

A loss less economic dispatch as opposed to a load flow solution is used in our algorithm to provide starting conditions for the full OPF solution. The equal incremental cost criterion is used for this purpose [19]. Different variants of this method are available in the open literature but the one we have adopted takes generators limits into consideration hence providing more realistic starting conditions.

5.3. Lagrange multipliers

The Lagrange multipliers for the active and reactive power flow mismatch equations are initialised at 1 and 0, respectively. For TCSC Lagrange multiplier the initial value of λ_{ml} is set to 0. It is our experience that this value gives rise to very robust iterative solutions.

5.4. TCSC's firing angle initial conditions

The main factor, which affects the OPF rate of convergence of TCSC-upgraded networks is the initial firing angle, α. Good starting conditions are required to avoid the solution diverging or arriving at some anomalous value. The initial condition for the TCSC's firing angle is selected within the range of ± 8 electric degrees away from the resonant point given by Eq. (5).

5.5. Implementation of the active power flow constraint

The implementation of the active power flow constraint requires careful consideration. Large variations in $\Delta\alpha$ take place in the early stages of the iterative process if the TCSC is set to control active power flow directly in the branch k–m. In this situation, the increments in the TCSC-FA are very large, leading to sudden changes from the capacitive to the inductive regions, causing the solution to diverge.

We have found that the OPF algorithm performs much more reliably when the active power flow is constrained at the sending node, m, of the compensated transmission line, m–l, i.e. the state variable α does not form part of Eq. (14).

We have also found that the limits revision of α should start taking place after the second iteration. Extensive testing has shown that this approach gives good iterative solutions, particularly when the voltage magnitude and active and reactive power limits have already been checked.

6. Test cases

The TCSC firing angle model, presented above, has been incorporated into our optimal power flow program. The objective function to be minimised is the active power generation cost. The OPF program has been applied to the solution of power networks of different sizes and some of them have been reported in the open literature [14,15]. The solutions given by our OPF algorithm compared favourably with published results in all cases.

6.1. 5-node network

A 5-node network is used first to quantify the TCSC behaviour in an interconnected network [20]. The reactance of the transmission line Lake-Main was increased from 0.03 to 0.04 p.u. in order to reach higher compensation levels, e.g. 30%. This transmission line was modified to incorporate one TCSC. The node Lake-TCSC was added to the network.

The TCSC firing angle model was used to optimise the active power flow level in transmission line Lake-Main, i.e. 14.97 MW, which is amenable to minimum active power generation costs and network losses, i.e. 747.975 $/h and 3.05 MW, respectively. The reactance values selected by the OPF algorithm to achieve this result are $X_C = 0.975\%$ and $X_L = 0.1625\%$, with respect to a base voltage of 400 kV. The solution was achieved in five iterations,

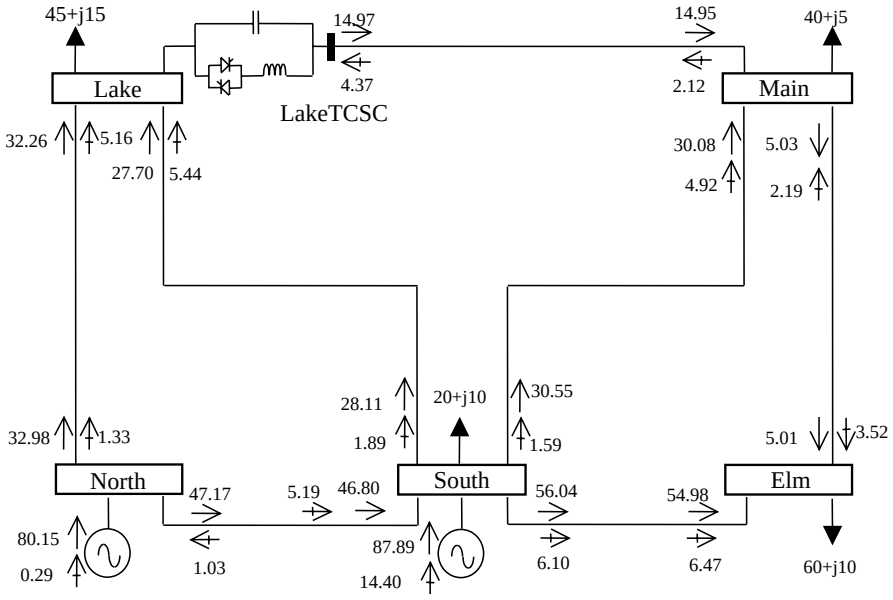

Fig. 4. Modified 5-node network and OPF solution.

starting from an initial firing angle of 150°. The resultant power flows are shown in Fig. 4 and the nodal voltages, Lagrange multipliers and active and reactive generated powers are given in Table 1. The firing angle and the TCSC reactance at each iteration are given in Table 2.

As expected, if the TCSC is set to regulate active power flow at a level different from the optimal value given by the OPF algorithm, then generation costs will rise. For instance, setting the power flow in transmission line Lake-Main at 10 MW leads to an active power generation cost of 748.072 $/h and the transmission losses are 3.072 MW. The solution was achieved in four iterations and the firing angle took a value of 141.75°. The solution takes place in the inductive region, 1° away from the resonant point.

6.2. Effect of the firing angle initial condition on the iterative solution

The choice of the TCSC's firing angle initial value has an important bearing upon the iterative process. This is investigated in this section.

The standard AEP14 node system [16], shown in Fig. 5, was modified to incorporate two TCSCs aiming at controlling active power flow across branches 5–4 and 12–13 at 30 and 2 MW, respectively. Furthermore, the inductive reactance of branch 12–13 was increased from 0.19988 to 0.24 p.u. in order to observe better the TCSC effects in this branch. In this situation, the power flows were 26.8 and 1.7 MW, respectively. For the purpose of this exercise, all the synchronous condensers in the original network were assumed to be synchronous generators, i.e. capable of generating active power. The data required by the optimisation algorithm, such as fuel cost curves, were given typical values.

In order to assess the impact of the firing angle initial guess, five different solutions were carried out. The first iterative solution was carried out with an initial firing angle of 144°. Subsequent solutions were performed with 3° increases with respect to the initial firing angle. Both TCSCs were initialised equally in every case. The TCSCs reactances are $X_C = 0.9375\%$. and $X_L = 0.1625\%$. It must be noted that the negative sign of the capacitive reactance has already been taken into account in Eq. (1).

In each case, all the inequality constraints were satisfied, except for the voltage magnitude at node 7, which was suitably enforced by means of the multiplier method. The number of iterations taken by the algorithm to converge to the specified tolerance was five for the first four cases. Exactly the same active power generation costs and active power losses were

Table 1
Nodal complex voltages of modified network

Node	Voltage magnitude (p.u.)	Phase angle (°)	Active power (MW)	Reactive power (MVAR)	λ_p ($/MW h)
Lake	1.078	−3.534	0	0	4.2232
TCSC					
Elm	1.072	−4.417	0	0	4.2639
Main	1.077	−3.846	0	0	4.2341
Lake	1.078	−3.622	0	0	4.2232
South	1.100	−1.303	87.89	14.40	4.1031
North	1.109	0.000	80.15	0.29	4.0412

Table 2
TCSC-FA parameters

Iterations	TCSC-FA parameters	
	α (°)	X_{TCSC} (p.u.)
0	150.000	−0.0180
1	150.587	−0.0169
2	162.845	−0.0101
3	154.328	−0.0130
4	156.399	−0.0119
5	156.407	−0.0119

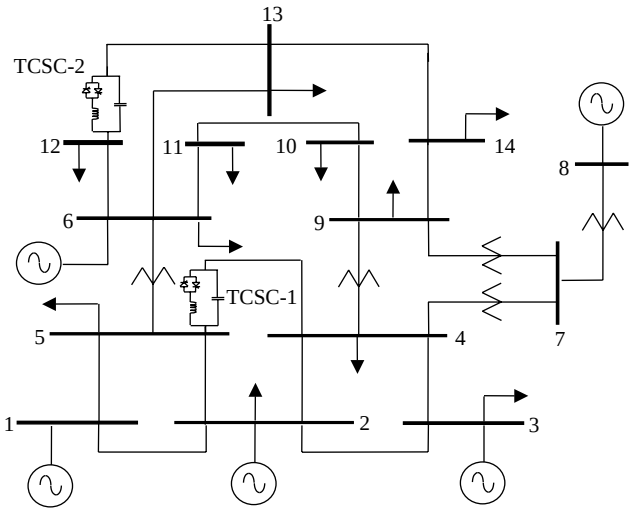

Fig. 5. AEP14 node system with two TCSCs.

arrived at, i.e. 215.453 $/h and 1.89968 MW. Similarly, the TCSC equivalent reactances were identical in all cases. The case for which the firing angle was initialised at 156° converged in four iterations but it converged to an undesirable value. The final TCSC's firing angles was very different than for the previous four cases. It settled down to 180°, which clearly indicates an unrealistic solution. Furthermore, the power generation costs and active power losses were much larger.

Figs. 6 and 7 show the firing angles profiles for both TCSCs as a function of iteration number. It can be observed that the patterns of convergence are highly irregular during the first global iteration. The very pronounced overshooting is due to the large variations taken place in the first and second derivatives of the TCSCs reactances with respect to the firing angles. It can be observed that the overshooting is reduced once the iterative process approaches the solution. Good initial conditions are amenable to small firing angle increments. Conversely, initial values far away from the solution, may lead to unrealistic answers. A case in point is the situation when the firing angle settles to a firing angle value of 180° for both TCSCs. This case corresponds to an

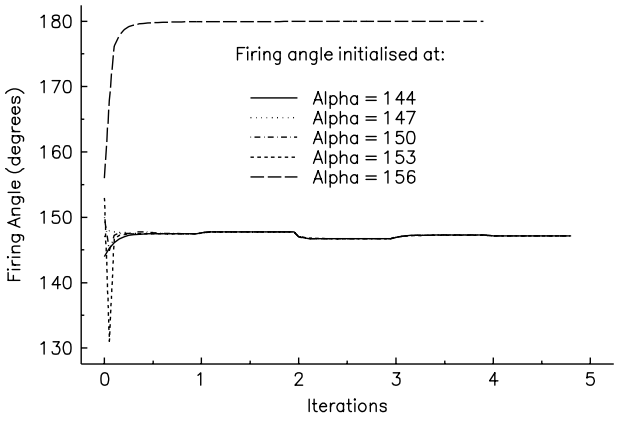

Fig. 6. TCSC-1 firing angle profile.

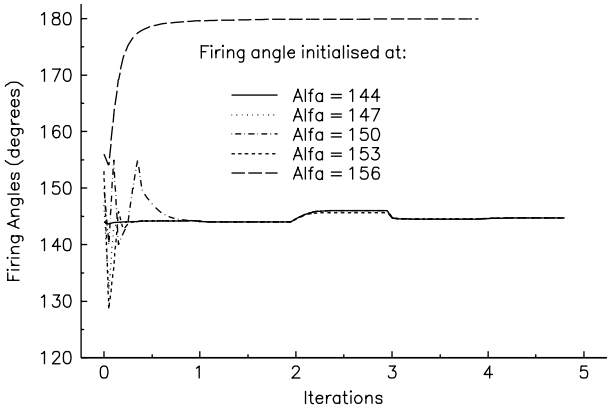

Fig. 7. TCSC-2 firing angle profile.

initial firing angle of 156°. It must be noted that in fact, from the beginning of the iterative solution the tendency is towards the 180°.

The very large perturbations taken place during the first global iteration lead to TCSC limits violations. Here, swaps from the capacitive to the inductive regions take place in a rather unpredictable manner. Hence, no attempt is made to revise TCSC limits before the end of the second global iteration. At this point, nodal voltages and active and reactive nodal power are revised and, if required, suitably enforced. It is our experience that from the second iteration onwards, the TCSC firing angle moves in a continuous and smooth fashion. The results above show that the algorithm is very robust towards the convergence; however, if unsuitable initial conditions for the firing angle are used then the algorithm will converge to an unrealistic value.

7. Conclusions

A new and more efficient TCSC-OPF model than those currently available in the open literature has been presented in this paper. The thyristor's firing angle, a newly introduced state variable in OPF formulations, is combined with the nodal voltage magnitudes and angles of the power network in a single frame-of-reference for unified iterative solutions via Newton's method. In this algorithm, the thyristor's firing angle is regulated in order achieve an optimal level of compensation under either condition, constrained or unconstrained power flow across the compensated branch. In the latter case, the power flow and compensation level are selected by the algorithm, leading to more economic solutions than in cases when the power flow is set to a specified value.

The extended OPF Newton algorithm has shown to be a very powerful tool, capable of solving TCSC-upgraded power networks very reliably, using a minimum of iterative steps. The computational efficiency of the OPF Newton algorithm is further tightened by using the multipliers method to handle the binding set, as opposed to the penalty functions method.

The task of finding suitable initial conditions for the thyristor's firing angle was found to be a troublesome issue, hence, it received a great deal of attention. The TCSC slopes

tend asymptotically to $\pm\infty$ at the resonant point and to zero at their maximum and minimum firing angle conduction points. These characteristics presented a challenge to the OPF Newton algorithm, which was successfully overcome. As expected, initial conditions far from the optimal firing angle may lead to anomalous solutions or may even cause the algorithm to diverge. Extensive testing has indicated that TCSC's firing angle of $+8°$ away from the resonant point provide good initial conditions for optimal iterative solutions taking place in the capacitive region, whereas an angle of $-8°$ away from the resonant point was suitable for solutions taking place in the inductive region.

The efficiency of the algorithm has been illustrated by numeric examples. Several networks of various sizes have been solved with the extended algorithm. Some of them correspond to large company networks. However, for the sake of presenting complete set of results, only two standard networks, suitably modified, are reported in the paper. These results clearly show the algorithm's flexibility and reliability towards the convergence.

Acknowledgements

The authors gratefully acknowledge the financial assistance given by the Consejo Nacional de Ciencia y Tecnología, México. Mr Ambriz-Pérez would like to thank Comisión Federal de Electricidad, México for granting him study leave to carry out PhD studies at the University of Glasgow, Scotland, UK.

Appendix A

The first and second partial derivative terms corresponding to the sending end of the TCSC are derived explicitly in this Appendix. These terms are obtained by deriving Eqs. (9) and (10) with respect to the firing angle. The first and second partial derivative terms for the receiving node are obtained by exchanging subscripts k and m in Eqs. (A1), (A2) and (A5)-(A15).

$$\frac{\partial P_k}{\partial \alpha} = -V_k V_m \sin(\theta_k - \theta_m) B_{TCSC}^2 \frac{\partial X_{TCSC}}{\partial \alpha} \tag{A1}$$

$$\frac{\partial Q_k}{\partial \alpha} = (-V_k^2 + V_k V_m \cos(\theta_k - \theta_m)) B_{TCSC}^2 \frac{\partial X_{TCSC}}{\partial \alpha} \tag{A2}$$

where

$$\frac{\partial X_{TCSC}}{\partial \alpha} = -2C_1[1 + \cos(2(\pi-\alpha))] + C_2 \sin(2(\pi-\alpha)) \times (\tan(\pi-\alpha) - \varpi \tan(\varpi(\pi-\alpha))) + C_2\left(\varpi^2 \frac{\cos^2(\pi-\alpha)}{\cos^2(\varpi(\pi-\alpha))} - 1\right) \tag{A3}$$

These equations are greatly simplified by incorporating the following relationship,

$$\cos(2(\pi-\alpha)) = \cos(2\alpha) \quad \text{and} \quad \sin(2(\pi-\alpha)) = -\sin(2\alpha) \tag{A4}$$

The second partial derivative terms of the power equations with respect to the firing angle are,

$$\frac{\partial^2 P_k}{\partial \alpha \partial V_k} = -V_m \sin(\theta_k - \theta_m) B_{TCSC}^2 \frac{\partial X_{TCSC}}{\partial \alpha} \tag{A5}$$

$$\frac{\partial^2 P_k}{\partial \alpha \partial V_m} = -V_k \sin(\theta_k - \theta_m) B_{TCSC}^2 \frac{\partial X_{TCSC}}{\partial \alpha} \tag{A6}$$

$$\frac{\partial^2 Q_k}{\partial \alpha \partial V_k} = (-2V_k + V_m \cos(\theta_k - \theta_m)) B_{TCSC}^2 \frac{\partial X_{TCSC}}{\partial \alpha} \tag{A7}$$

$$\frac{\partial^2 Q_k}{\partial \alpha \partial V_m} = V_k \cos(\theta_k - \theta_m) B_{TCSC}^2 \frac{\partial X_{TCSC}}{\partial \alpha} \tag{A8}$$

$$\frac{\partial^2 P_k}{\partial \alpha \partial \theta_k} = -V_k V_m \cos(\theta_k - \theta_m) B_{TCSC}^2 \frac{\partial X_{TCSC}}{\partial \alpha} \tag{A9}$$

$$\frac{\partial^2 P_k}{\partial \alpha \partial \theta_m} = V_k V_m \cos(\theta_k - \theta_m) B_{TCSC}^2 \frac{\partial X_{TCSC}}{\partial \alpha} \tag{A10}$$

$$\frac{\partial^2 Q_k}{\partial \alpha \partial \theta_k} = -V_k V_m \sin(\theta_k - \theta_m) B_{TCSC}^2 \frac{\partial X_{TCSC}}{\partial \alpha} \tag{A11}$$

$$\frac{\partial^2 Q_k}{\partial \alpha \partial \theta_m} = V_k V_m \sin(\theta_k - \theta_m) B_{TCSC}^2 \frac{\partial X_{TCSC}}{\partial \alpha} \tag{A12}$$

$$\frac{\partial^2 P_k}{\partial \alpha^2} = -V_k V_m \sin(\theta_k - \theta_m) \times \left(B_{TCSC}^2 \frac{\partial^2 X_{TCSC}}{\partial \alpha^2} + \frac{\partial X_{TCSC}}{\partial \alpha} \frac{\partial B_{TCSC}^2}{\partial \alpha}\right) \tag{A13}$$

$$\frac{\partial Q_k}{\partial \alpha} = (-V_k^2 + V_k V_m \cos(\theta_k - \theta_m)) \times \left(B_{TCSC}^2 \frac{\partial^2 X_{TCSC}}{\partial \alpha^2} + \frac{\partial X_{TCSC}}{\partial \alpha} \frac{\partial B_{TCSC}^2}{\partial \alpha}\right) \tag{A14}$$

$$\frac{\partial B_{TCSC}^2}{\partial \alpha} = -\frac{2}{X_{TCSC}^3} \frac{\partial X_{TCSC}}{\partial \alpha} \tag{A15}$$

$$\begin{aligned}\frac{\partial^2 X_{TCSC}}{\partial \alpha^2} = {} & -4C_1 \sin(2(\pi-\alpha)) \\ & + C_2 \varpi^2 \left[\frac{2\cos^2(\varpi(\pi-\alpha))\cos(\pi-\alpha)\sin(\pi-\alpha)}{\cos^4(\varpi(\pi-\alpha))}\right] \\ & - C_2 \varpi^2 \left[\frac{2\varpi\cos^2(\pi-\alpha)\cos(\varpi(\pi-\alpha))\sin(\varpi(\pi-\alpha))}{\cos^4(\varpi(\pi-\alpha))}\right] \\ & + C_2 \varpi \left[2\tan(\varpi(\pi-\alpha))\cos(2(\pi-\alpha)) + \frac{\varpi \sin(2(\pi-\alpha))}{\cos^2(\varpi(\pi-\alpha))}\right] \\ & - C_2 \left[2\tan(\pi-\alpha)\cos(2(\pi-\alpha)) + \frac{\sin(2(\pi-\alpha))}{\cos^2(\pi-\alpha)}\right]\end{aligned} \tag{A16}$$

References

[1] Fuerte-Esquivel CR, Acha E. A Newton-type algorithm for the control of power flow in electrical power networks. IEEE Trans Power Deliv 1997; 2(4):1474–80.

[2] Hingorani NG. Flexible AC transmission systems. IEEE Spectr 1993; 30(4):40–5.

[3] IEEE Power Engineering Society. FACTS applications. Special issue, 96TP116-0. IEEE Service Center, Piscataway, NJ; 1996.

[4] Christl N, Hedin R, Johnson R, Krause P, Montoya AA. Power system studies and modelling for the Kayenta 230 kV substation advance series compensation. Proceedings of IEE 5th international conference on AC and DC power transmission; 1991. p. 33–7.

[5] Gama C, Salomao JCS, Gribel JB, Ping W. Brazilian north–south interconnection—application of thyristor controlled series compesator (TCSC) to damp inter-area oscillation mode. Proceedings of EPRI conference on the future of power delivery in the 21st century, session 2–grid operation and planning; 1997.

[6] Helbing SG, Karady GG. Investigations of an advanced form of series compensation. IEEE Trans Power Deliv 1994;9(2):939–47.

[7] Tenorio ARM, Jenkins N, Bollen MHJ. A TCSC model for electromagnetic transient studies. Proceedings of IEEE/KTH stockholm power tech conference; 1995. p. 130–5.

[8] Piwko RJ, Wegner CA, Kinney SJ, Eden JD. Subsynchronous resonance performance tests of the slatt thyristor-controlled series capacitor. IEEE Trans Power Deliv 1996;11(2):1112–9.

[9] Wang HF, Swift FJ. A unified model for the analysis of FACTS devices in damping power system oscillations part I: single-machine infinite bus power system. IEEE Trans Power Deliv 1997;12(2):941–6.

[10] Hedin R, Jalali S, Weiss S, Cope L, Johnson B, Mah D, et al. Improving system stability using an advanced series compensation scheme to damp power swings. Proceedings of IEE 6th international conference on AC and DC power transmission; 1996.

[11] Taranto GN, Pinto LMVG, Pereira MVF. Representation of FACTS devices in power system economic dispatch. IEEE Trans Power Syst 1992;7(2):572–6.

[12] Sun DI, Ashley B, Brewer B, Hughes A, Tinney WF. Optimal power flow by Newton approach. IEEE Trans Power App Syst 1984;103(10): 2864–80.

[13] Sun DI, Hu TI, Lin GS, Lin CJ, Chen CH. Experiences with implementing optimal power flow for reactive scheduling in the Taiwan power system. IEEE Trans Power Syst 1988;3(3):1193–200.

[14] Divi R, Kesavan JA. A shifted penalty function approach for optimal load-flow. IEEE Trans Power App Syst 1982;101(9):3502–12.

[15] Wu QH, Ma JY. Power system optimal reactive power dispatch using evolutionary programming. IEEE Trans Power Syst 1995;10(3):1243–9.

[16] Freris LL, Sasson AM. Investigation of the load-flow problem. Proc IEE 1968;115(10):1459–70.

[17] Luenberger DG. Introduction to linear and nonlinear programming. 2nd ed. Reading, MA: Addison Wesley; 1984.

[18] Bertsekas DP. Constrained optimization lagrange multiplier methods. New York: Academic Press; 1992.

[19] Wollenberg B, Wood AJ. Power generation, operation and control. 2nd ed. New York: Wiley; 1984.

[20] Stagg GW, El-Abiad AH. Computer methods in power system analysis. 10th printing. New York: McGraw-Hill; 1968.

H. Ambriz-Pérez was born in México in 1964. He received his BEng degree (Hons) and his MSc degree from Instituto Politécnico Nacional, México in 1987 and 1992, respectively. He obtained his PhD degree from the University of Glasgow, Scotland, UK in 1999. He is currently at the Specialised Engineering Unit of Comisión Federal de Electricidad at México City.

E. Acha graduated from University of Michoacán in 1978 and obtained his PhD degree from the University of Canterbury, Christchurch, New Zealand in 1988. He was a postdoctoral fellow at the Universities of Toronto, Canada and Durham, England. He holds the position of Professor at the University of Glasgow, Scotland, where he lectures and conducts research on power systems analysis and power electronics applications.

C.R. Fuerte-Esquivel received his BEng degree (Hons) from Instituto Tecnológico de Morelia, México in 1990, his MSc degree from Instituto Politécnico Nacional, México in 1993 and his PhD degree from the University of Glasgow, Scotland, UK in 1997. He is currently with the División de Estudios de Posgrado of the Facultad de Ingeniería Eléctrica, UMSNH, Morelia, Michoacán. His current interests are the steady-state and dynamic modeling and analysis of FACTS.